



UNIVERSITY OF LEEDS

This is a repository copy of *In situ characterization of mixing and sedimentation dynamics in an impinging jet ballast tank via acoustic backscatter*.

White Rose Research Online URL for this paper:
<http://eprints.whiterose.ac.uk/113005/>

Version: Accepted Version

Article:

Bux, J, Paul, N, Peakall, J et al. (3 more authors) (2017) In situ characterization of mixing and sedimentation dynamics in an impinging jet ballast tank via acoustic backscatter. *AIChE Journal*, 63 (7). pp. 2618-2629. ISSN 0001-1541

<https://doi.org/10.1002/aic.15683>

(c) 2017, American Institute of Chemical Engineers (AIChE). This is the peer reviewed version of the following article: "Bux, J, Paul, N, Peakall, J et al (2017) In situ characterization of mixing and sedimentation dynamics in an impinging jet ballast tank via acoustic backscatter. *AIChE Journal*," published in final form at [<https://doi.org/10.1002/aic.15683>]. This article may be used for non-commercial purposes in accordance with Wiley Terms and Conditions for Self-Archiving.

Reuse

Unless indicated otherwise, fulltext items are protected by copyright with all rights reserved. The copyright exception in section 29 of the Copyright, Designs and Patents Act 1988 allows the making of a single copy solely for the purpose of non-commercial research or private study within the limits of fair dealing. The publisher or other rights-holder may allow further reproduction and re-use of this version - refer to the White Rose Research Online record for this item. Where records identify the publisher as the copyright holder, users can verify any specific terms of use on the publisher's website.

Takedown

If you consider content in White Rose Research Online to be in breach of UK law, please notify us by emailing eprints@whiterose.ac.uk including the URL of the record and the reason for the withdrawal request.



eprints@whiterose.ac.uk
<https://eprints.whiterose.ac.uk/>

***In situ* characterization of mixing and sedimentation dynamics in
an impinging jet ballast tank via acoustic backscatter**

Jaiyana Bux*, Neepa Paul, Jeffrey Peakall, Timothy N. Hunter**

School of Chemical & Process Engineering

**School of Earth and Environment

University of Leeds, Leeds, West Yorkshire, LS2 9JT, UK

Jonathan M. Dodds

National Nuclear Laboratory, Central Laboratory, Sellafield, Cumbria CA20 1PG, UK

Simon Biggs

School of Chemical Engineering,

The University of Queensland, Brisbane, Queensland QLD 4072, Australia

* Corresponding author email: J.Bux@leeds.ac.uk

This article has been accepted for publication and undergone full peer review but has not been through the copyediting, typesetting, pagination and proofreading process which may lead to differences between this version and the Version of Record. Please cite this article as doi: 10.1002/aic.15683

© 2017 American Institute of Chemical Engineers (AIChE)

Received: Sep 26, 2016; Revised: Feb 08, 2017; Accepted: Feb 13, 2017

Abstract

Impinging jets are utilized in numerous applications, including nuclear waste treatment, for both the erosion of sediment beds and maintaining particulates in suspension. Pulse-echo ultrasonic methods offer great potential for the *in situ* monitoring of critical mixing and settling dynamics, in concentrated dispersions. A non-active scaled version of a Highly Active Storage Tank at Sellafield, UK, was profiled with an acoustic backscatter system under various jet firing conditions. An advanced analysis technique enabled the direct quantification of dispersion concentration changes from the converted backscatter attenuation. Hence, the erosion and mixing capability of the jets, and settling kinetics were characterized. It was found that jet operation alone provided inadequate localized mixing of eroded sediment. An additional air-lift process operation was required to hinder the rapid re-settling of dispersed particulates.

Particle Technology and Fluidization

Keywords

acoustic backscatter, impinging jets, erosion, sedimentation, fluid mixing

Introduction

Understanding mixing and segregation dynamics in multiphase dispersions, suspensions and slurries is of ubiquitous importance within many chemical engineering processes, ranging from pharmaceutical, personal care, cosmetics, pigments and food manufacture,¹ to large scale multiphase separation processes in fuels, minerals processing and water treatment.² A particularly challenging example is the use of multiphase mixing systems for nuclear waste treatment and transfer across the US, UK and Europe, where jet ballasts are utilized to homogenize settled materials such as radioactive suspensions, due to their increased reliability in comparison to mechanical mixers.^{3,4} The process involves eroding and mobilizing sludge waste layers via jet impingement, where consequential liquid turbulence disperses particles into suspension.^{4,5}

It is critical from operational and optimization perspectives, to have an understanding of dispersion dynamics in such jet systems; specifically on particle erosion,⁶ mobilization and mixing, as well as settling kinetics, particulate segregation and concentration changes once jets are stopped.⁷ Yet, such dynamic information is not easily acquired at full scale or via *in situ* characterization techniques, and is often estimated from lab scale mixing or settling tests, where results may be correlated to real systems by labor intensive sampling of particle concentrations or radioactivity over time. Indeed, many jet-erosion systems rely on theoretical models to overcome experimental difficulties with the prediction of process behavior.⁸ Nevertheless, numerical simulations of erosion via impinging jets are still at an early stage⁹ and thus it is imperative that experimental techniques are developed to allow current models to correlate prediction with real system data.^{7,10}

A range of *in situ* devices are available for suspension monitoring that may be applied to such fast jet mixing systems: For example, light transmission or backscattering devices,¹¹⁻¹³ x-ray¹⁴ and gamma ray transmission,¹⁵ laser induced fluorescence,^{7,10,16} CCD video analysis,¹⁷ and tomographic methods measuring electrical resistance.¹⁸ However, many of these techniques also contain limitations that have reduced their more wide scale industrial use including, low particle concentration thresholds, high intrusiveness, high cost or implementation complexity.¹⁹ Ultrasonic diagnostics however, can surmount many of these issues to a practicable extent,² and offer improved flexibility and fast sampling rates for the monitoring of particle size, concentration and velocity in dynamic dispersions.²⁰⁻²⁶ Specifically, acoustic backscatter systems (ABS), have been demonstrated for the characterization of suspended sediment concentration (SSC) and particle sizing in dilute estuarine flows of coarse sediments,^{27,28} fine sediments,²⁹ colloidal dispersions,^{30,31} concentrated suspensions and for the tracking of settling interfaces.^{26,31-36}

Thorne and Hanes²⁸ developed a model for SSC characterization of dilute sandy sediments which applies only to particle sizes greater than 40 μm , concentrations below approximately 2.5 g/l,³² and requires independent knowledge of particle specific scattering and attenuation constants which are determined from the corresponding form functions and total normalized scattering cross sections; these are only readily available in literature for large glass beads and sandy particles.³⁷⁻³⁹ Hunter *et al.*³² and Bux *et al.*,³¹ outlined a phenomenological approach, whereby in cases where there is a linear decay in the backscattered signal on the decibel scale, the attenuation gradient can be correlated directly with concentration. This approach enables the characterization of concentration and settling kinetics in dispersions

comprising arbitrary particle types, because predetermined knowledge of particle properties isn't a prerequisite, and in higher concentration regimes than the Thorne and Hanes model,²⁸ due to the corresponding linearity of the signal decay. Rice *et al.*²² presented an advanced analysis method, which enables the calculation of the attenuation constants of arbitrary particles directly from backscatter measurement, negating the need for laborious defining of the total normalized scattering cross-section.

The Rice method²² rearranges the Thorne and Hanes²⁸ expression for backscattered voltage in terms of the *G-function*: $[G = \ln(\psi Vr)]$, where V is the backscattered voltage, r is the transducer distance range and ψ is a near-field correction factor that can theoretically account for response variation at short distances.⁴⁰ It was shown by Rice *et al.*²² that for a well-mixed dispersion, G varies linearly with distance r , and that more importantly, the gradient of the *G-function*, $\partial G/\partial r$ varies linearly with particle concentration. The *Rice method*²² enables quantification of sediment concentration in many particle systems across a wide range, using the gradient equation; $[\xi = -1/2 \partial G/\partial r]$, where ξ is the sediment attenuation constant, to generate particle specific correlations. A derivation of the *G-function* is available in the Supplementary Material section, S1. Importantly, in the *G-function* model, gradient linearity holds for a larger concentration range than the phenomenological correlation method,^{31,32} where the influence of inter-particle scattering becomes so enhanced, at a limiting concentration, that the signal decay is no longer linear on a decibel scale.

In this report, we investigate the application of an acoustic backscatter system (ABS) utilizing a combined analysis approach for the first time, which incorporates the *Rice method*²² alongside the phenomenological approach,^{31,32} to characterize concentration and dispersion kinetics, within a large scale impinging jet mixing tank.

Specifically, a tank system from the UK nuclear industry is investigated, where the characterization of legacy waste sludges pending retrieval from aged tanks and silos is very challenging.⁴¹ Highly Active Storage Tanks (HASTs) are utilized by Sellafield Ltd UK, for the interim storage of the penultimate liquid waste stream arising from spent nuclear fuel reprocessing. They comprise impinging jet ballasts to erode and re-suspend fission products that have precipitated out of solution and settled onto the tank base.^{41,42} HASTs also incorporate heat exchange cooling coils to remove residual radioactive decay heat. These occupy a significant tank volume, thus undesirable particulate sedimentation onto this pipework is also known to occur⁴¹. Furthermore, air-lifts are also incorporated in the design. These generate additional turbulence in order to improve mixing of dispersed sediment. It is critically important to understand the level of mixing achieved both with and without air-lift operation.

Monitoring suspension conditions is a significant challenge within the HASTs owing to the inherent radioactivity and their congested internal structure. Hence, the availability of practical *in situ* characterization instrumentation is imperative. Direct deployment of an ABS in the HASTs was not practical for this preliminary investigation, owing to the high radioactivity. Instead, non-active test experiments were conducted in a four tenths scale rig with the aim of correlating suspension behavior within HASTs using current models.⁴² Specifically; the clearance achieved via erosion, levels of sediment mixing and dispersion, sediment re-settling and the influences of neighboring jets, were investigated by employing various jet and air-lift operating regimes. An inorganic mineral comprising settling properties corresponding with a 40% scaling of active sludge solids, was utilized to model particulate behavior in these non-active trials. The sediment was calibrated in the laboratory to extract the unique relationship between *G-function* attenuation and concentration. This was

utilized as a reference to quantify concentration from measured backscatter in the FTR trials. Sedimentation tests were also conducted in the laboratory to gauge expected settling behavior, prior to non-active trials.

Experimental

Materials

The selection of materials that can be utilized in large scale experiments is typically limited due to practicality, toxicity and cost. Barium sulfate or barytes (supplied from RBH Ltd UK), was selected as the non-radioactive test material in the corresponding experiments, because it enables investigation of settling properties in a scaled scenario. Barytes is highly dense, akin to cesium phosphomolybdate (CPM) and zirconium molybdate (ZM), the primary constituents of HAST waste liquors.⁴¹

Material density was measured via a Micrometrics Accu-Pyc 1330 helium pycnometer (Micrometrics Instrument Corporation, USA). Three individual powder samples were measured three times each, yielding a density value of 4418 kgm^{-3} , which is close to the reference value of 4490 kgm^{-3} .⁴³ The measured density is higher than that of CPM (3820 kgm^{-3}) and ZM (3410 kgm^{-3})⁴¹, enabling experimental investigation of a worse case settling scenario for modeling purposes.

Particle size distribution was measured via a Malvern Mastersizer 2000 laser diffractometer (Malvern Instruments, UK), where three samples were dispersed in water, recirculated at 1400 rpm and measured ten times each (Figure 1). The distribution is bimodal with a primary peak at $10 \mu\text{m}$ and a minor volume fraction of fines at $1 \mu\text{m}$. The resulting D_{10} , D_{50} and D_{90} percentile diameters are 1.7, 7.8 and $18.7 \mu\text{m}$, respectively. In addition, three powder samples were imaged with a

LEO/Zeiss 1530 FEGSEM scanning electron microscope (LEO Elektronike GmbH, Germany) (Figure 2). These images both corroborate the laser diffractometer measured particle size, as well as revealing the shape characteristics, which in this case are non-uniform crystalline structures with uneven fractured flat faces. Size and shape both require consideration because not only do they influence settling behavior, but they also govern the backscatter response of the acoustic wave; whereby small particle radii, non-spheroidal shape and orientation in dispersion can enhance backscatter attenuation.⁴⁴ Although barytes is larger than colloidal CPM and ZM, it is at least an order of magnitude smaller than large sandy sediments that are characterized in typical marine ABS applications.²⁷ The stability of barytes in aqueous dispersions was also characterized via ζ potential measurement, using the Zetasizer Nano-ZS (Malvern Instruments, UK). A minimum of three samples were measured, with each sample comprising a maximum of 100 measurement runs.

Laboratory calibration & settling methodology

A 0.3 x 0.8 m Perspex column with inset baffles was utilized for the calibration of the barytes sediment (Figure 3). The column was fitted with an off-centered mixing impeller that was positioned 0.1 m from the base and mixing at a rate of 1640 rpm. Three transducers; 1 x 1 MHz and 2 x 2 MHz, were utilized with an AQUAScat 1000 acoustic backscatter system (Aquatec Group Ltd, UK), positioned at 0.55 m from the base to ensure sufficient submersion below the waterline at 0.60 m. Barytes sediment was dispersed in tap water to correspond with the solids settling properties. Suspension concentration was increased incrementally from 0.06 to 1.42 vol% with a 10 minute homogenization period between sediment addition and acoustic measurement. The transducers profiled the suspensions for a duration of 5 minutes, pulsing in sequence at a rate of 32 Hz, storing 1 averaged profile per second in 2.5

mm distance bins. Three runs were conducted per concentration, and an averaged backscatter intensity profile was ascertained per concentration. Three 50 ml samples were extracted, using a peristaltic pump, from four equidistant depths at the highest concentration for a homogeneity check. Depth-wise suspension homogeneity was confirmed with standard deviation ranging ± 0.001 – 0.044 vol%, as seen in Figure 4.

The settling tests were conducted via an analogous method, albeit with minor alterations; the waterline was set at 0.4 m and mixing impeller speed at 1200 rpm.

The settling of a suspension with bulk concentration of 0.7 vol% (~3 wt%) was investigated to match the nominal concentration in the industrial experiments. The transducers were positioned at 0.25 m to enable profiling within the sediment bed region. The dispersion was mixed for 10 minutes post sediment addition to ensure homogeneity, after which the mixer was turned off and the settling dispersions were profiled for a duration of 10 minutes. Three experimental runs were conducted per concentration, between which 10 minute mixing intervals were allowed for re-dispersion and homogenization of sediment.

Industrial impinging jet tank system

The Four Tenths Rig (FTR) at the National Nuclear Laboratory (Workington, UK) was utilized for non-active industrial experimental trials. The FTR, which is pictured in the Supplementary Material S2, is a 40% scaled version of a Highly Active Storage Tank (HAST), of the type at Sellafield Ltd (Cumbria, UK).⁴² The HAST is a storage vat which routinely mobilizes radioactive liquor waste, to prevent settled particles forming radioactive hotspots. The FTR design comprises three primary features; impinging jet ballasts to resuspend and mobilize settled particles, 'dummy' cooling coils to remove radioactive decay heat and air-lifts to generate turbulence and enhance particle mixing. The FTR is a Perspex column, 2.5 m in height and 2.6 m in

diameter, which is supported on a platform. At 100% fill, the FTR contains 12.10 m^3 of water generating a waterline height of 2.28 m from the base, or 1.44 m at 50% fill.

Experiments were conducted at both fill levels. The jet arrangement consists of six equidistant peripheral jets and a central jet with a vertically positioned nozzle. The central jet nozzle is positioned 0.38 m above the base, and the peripheral jet nozzles are angled towards the wall and positioned 0.23 m above the base. These features are visualized in schematics in Figure 5; (A) plan view, (B) CAD schematic of internal structure, and (C) side view of experimental configuration.

Jet ballasts withdraw fluid from the FTR and fire it out at a known velocity, creating an impingement which erodes the sediment bed to resuspend settled particles. At 40 Hz pump operating frequency, the jet nozzle diameters of 0.015 m, limit the maximum flowrate of the central jet to 230 l/min, and 196 l/min for the peripheral jets. During operation, each jet's velocity profile increases, reaches a plateau and then eventually decreases. A typical jet velocity profile with respect to time is provided in the Supplementary Material, S3, for reference. There are also four air-lift pipes which comprise perforated dispersion nozzles. The upper and lower positions of the nozzles are 0.21 m and 0.07 m respectively, from the base. They inject air into the suspension at a rate of 4 l/s and 1 bar_g pressure, to promote mobilization and homogenization of suspended particles.

The AQUAscat 1000 ABS (Aquatec Group Ltd, UK) was deployed here initially with 1 x 1 MHz and 1 x 2 MHz transducers. The 1 MHz transducer was positioned approximately 0.8 m from the base to monitor large depth scale suspension changes, due to its enhanced depth penetration compared with the higher frequencies. The 2 MHz transducer which is relatively more sensitive, was positioned approximately 0.3 m from the base to capture developments within the near-base

region. Consequently, the probes were not co-located. The 1 MHz was positioned closer to jet 2, and 2 MHz closer to jet 3 (Figure 5). The region between jets 2 and 3 was the only access point free from internal coils to enable ABS measurement. The highest transducer pulse repetition rate (64 Hz) was selected and one full depth profile was collected every second, to reduce the influences of noise. The depth profiles were segregated into 5 mm measurement bins to enable maximum depth penetration without compromising depth-wise resolution.

A range of HAST operation cycles were replicated in the FTR, in order to better understand sediment erosion and mobilization dynamics from an operational perspective. These are detailed in Table 1. Specifically, in Regime 1 (R1), only jet 1 and the central jet were operated. This regime was selected to investigate sediment mobilization influences of neighboring jets, and is analogous to experimental regimes selected by Hunter *et al.*,³ in a small scale 1 m³ tank without internal cooling coils. Regime 2 (R2), where each of the jets are operated in sequence, is more similar to a typical daily HAST mobilization operation. In Regime 3 (R3), all air-lifts are operated simultaneously with the jet cycle, to generate turbulence and thus promote mixing and homogenization of particles resuspended by the jets. The air-lift operation ceases upon completion of the jet firing cycle. This sequence resembles a typical operation that is conducted prior to HAST decantation, where liquor suspensions are pumped out for vitrification. ABS measurements commenced upon firing of the final jet in each regime and ceased by 30 minutes post firing. 60 minute inoperative periods between experiments were used to enable sediment to resettle close to background levels. ABS readings were taken 60 minutes post operation, in order to establish background concentration levels. Note, variations in firing time cycles is a capability of the FTR, which enables investigation of the direct influences of a range

of operational variables. These variables are not necessarily adjustable to the same extent in an actual HAST.

Regime 3 experiments were conducted with an additional 2 MHz probe co-located with the 1 MHz to profile changes in the corresponding upper-region. As part of the Regime 3 experiments, tank validation of the ABS concentration measurements was undertaken using independent sampling. Sampling was initiated post firing of jet 2 in the second cycle, i.e. 30 s prior to cycle completion. 2 x 20 ml samples were extracted with a peristaltic pump at selected times, at 0.15 m from the base. For each jet in Regime 3 experiments, and for the central jet in Regime 2 experiments, bed clearance profiles were measured, through the underside of the transparent rig. The equilibrium clearance area was then calculated for each jet.

Results and Discussion

Laboratory calibration

Averaged backscatter profiles of homogenous dispersions in the laboratory calibration tests, ranging 0.06–1.42 vol%, are presented in Figure 6 in terms of the *G-function* [$G=\ln(\psi Vr)$], with respect to transducer range. Note, for figure clarity, only data from three concentrations are shown, which broadly cover the range measured. The intense peak in backscatter intensity at 0.5 m denotes the tank base position relative to the transducers. The *G-function* backscatter intensity is strongest at the closest range and progressively attenuates due to natural absorption losses. This extinction in echo intensity, is enhanced for the 2 MHz frequency due to the shorter pulse wavelength.⁴⁵ Attenuation is also further pronounced with increasing concentration, due to the inherently augmented occurrence of inter-particle

scattering events which deviate the echoes from their path to the transducer.^{31,32} The data between transducer range 0.1 m and 0.4 m, or up until the signal threshold denoted by the minimum at 1.42 vol% for example, were utilized in subsequent data analysis.

The *G-function* profiles exhibit a linear extinction with respect to r , in this range, which enables direct quantification of attenuation with respect to concentration, where the attenuation constant is, $\zeta = -\frac{1}{2} \partial G / \partial r$, as per the *Rice method*.²² Accordingly, the averaged linear gradient of the *G-function* profiles were measured in the far-field (dashed lines in Figure 6.) for each transducer and system, and these values (representing $\partial G / \partial r$) are plotted against particle concentration in Figure 7. Importantly, Figure 7 confirms a linear relationship between $\partial G / \partial r$ and M , for concentrations > 0.1 vol%, and therefore it was utilized as a reference relationship for the direct inference of barytes concentration from the measured *G-function* backscatter, in the subsequent four tenths scale jet testing.

The values of the attenuation constants ' ζ ' are; 0.1254, 0.1910 and 0.1867 kg^{-1}m^2 for 1 MHz, 2 MHz (probe 1) and 2 MHz (probe 2) respectively. These values indicate that barytes sediment attenuates the backscattered pulse far more than larger glass bead and jagged plastic particles that have been previously investigated.²² This is primarily due to their correspondingly smaller size range, where viscous absorption of the acoustic pulse is high.⁴⁴ The consistency between the two 2 MHz calibrations is in agreement with theory since $\partial G / \partial r$ should not show significant deviation between transducers, as it should be entirely a material property.

Laboratory study of barytes settling

Figure 8A presents the average backscatter profiles obtained at selected time intervals (in minutes), in the laboratory settling investigation of a 0.7 vol% barytes dispersion. For data analysis, it was found that further averaging of adjacent one second time profiles was required to reduce the influence of random fluctuations in data, due to inherent signal noise generated in this dynamic settling system. Five second time averaging was found to be optimal and thus selected for analysis. Averaging over smaller durations proved noisy, whereas averaging over greater durations proved too long a time frame, with respect to the sedimentation dynamics of the system. The five second averages adopted here were also found to be optimal time frames using the same instrument in dynamic settling sludge suspensions.^{31,34} Hence, the profiles in Figure 8A, represent five second averaged results measured via the 2 MHz transducers, akin to previous investigations of similar settling systems.³¹ Initially, T(0) (time in minutes), depicts an intense narrow peak at 28.25 cm, which denotes the column base position relative to the transducer. In subsequent time profiles, the peak recedes in intensity and shifts towards the transducer. This shift is indicative of a bed interface, where sediment is deposited at the base. The final bed depth at T (10) is 0.75 cm.

An additional broader peak is observed close to the transducer, positioned at 7.5 cm in profile T(2), as denoted by the arrow. The peak successively shifts towards the column base, as seen in profiles T(3) and T(3.5) (arrows). These features are indicative of a settling dispersion, where the moving broad peaks corresponds with the demarcation of a diffuse clarified supernatant – settling suspension boundary.^{31,33,34} The positions of the settling front and sediment bed were measured over successive time profiles and plotted in Figure 8B. Note, data were not included in the region of 4 minutes due to difficulty encountered in defining the exact position

of the very diffuse settling front – bed boundary, at this point in time. The resulting sedimentation curve indicates the occurrence of hindered settling behavior in the 0.7 vol% dispersion, the settling rate of which is 1.35 mm/s at suspension temperature 24.5°C. The average ζ potential corresponding with the dispersion at pH 7 ranges 0.4 – 3.2 mV. Low magnitude ζ potential data indicate weak electrostatic repulsion forces between particles, which are insufficient to prevent aggregation.⁴⁶ Indeed, the measured settling rate is considerably faster than the Stokes free settling velocity of 0.51 mm/s for 7.8 μm particle size. These results suggest that the particles may be aggregating in suspension. Indeed, fine cohesive minerals are known to aggregate in suspension and exhibit complex settling behavior.⁴⁶ A transition from the individual deposition of barytes aggregates to hindered settling behavior, has previously been reported to be in the region of 1 vol% concentration.⁴⁷

Suspension concentration within the settling regions (between the broad settling peak and bed peak for selected time profiles in Figure 8A) were characterized via the reference relationship determined from the calibration experiment discussed in the previous section. Backscatter profiles in Figure 8A, were subsequently averaged over 5 successive time profiles (5 s), and plotted in terms of the *G-function* versus transducer range, akin to the calibration methodology. The gradients ($\partial G/\partial r$), were calculated in successive 5 distance bin segments, over the corresponding profile range, for each examined profile. The value of $\partial G/\partial r$ for each segment was then quantified in terms of concentration via the calibration reference given in Figure 7. The corresponding depth-wise concentration profiles are presented in Figure 9 A to D, over four time profiles in minutes. The dispersions are fairly homogeneous initially, around the expected bulk concentration zone, demonstrating good correlation between the reference relationship and measured initial volume fraction

set-up within the tank. Profiles A and B do however show significant variations suggesting an error of ± 0.1 vol%, or around $\sim \pm 10\%$ relative. Considering the fast settling kinetics that are occurring in these systems, which limits the data capture time, such variation is considered acceptable for the required jet tank studies, and is consistent with previous ABS studies of settling suspensions.^{31,34} Figure 9 C and D, also show that a concentration gradient from the settling interface to the near-bed progressively develops with time. Generally, particles of different sizes settle at different rates in polydisperse suspensions,⁴⁷ and given that barytes is bi-disperse in this case, size segregation during settling is the likely cause for the profiled concentration changes observed. It is evident that detailed information is obtained on the settling kinetics of the bidisperse suspension via the ABS, with the instrument giving the ability to not only monitor interfacial changes but particle segregation through concentration in the same measurement.

Sediment erosion in the impinging jet Four Tenths Rig (FTR)

Bed clearance dimensions were measured from the underside of the transparent tank post Regime 3 jet-only operation, in order to gauge the erosion capability of the jets. Clearance was also measured for the central jet post Regime 2, where the corresponding jet was fired in sequence rather than continuously throughout the cycle, to gauge jet duration influences. Visual inspection of the tank underside, revealed that the clearance pattern of the peripheral jets were not as uniform as the expected empirical clearance model generated by McArthur *et al.*,⁴² as shown in Figure 10A. This is because the peripheral jet nozzles are angled at the tank wall, creating effectively a double impingement. Figure 10C, illustrates how the liquid jet initially impinges on the vertical wall (solid blue lines), spreads along the wall to the tank base (dotted blue lines), secondarily impinging at the tank corner. Thus, a lot

more of the jet energy is directed along the tank wall, rather than out into the bed, which tended to create a semi-ellipsoidal erosion profile in an outward direction from the wall - base boundary (dashed blue line). In actuality, the peripheral jets generated a non-uniform clearance area, due likely to inhomogeneous bed yield-strength, the approximate shape of which is depicted in Figure 10B.

The procedure for quantifying peripheral clearance areas is outlined henceforth. The measured major and minor axis dimensions are given in Table 2. In almost all cases, the minor axis is not directly half the value of the major axis, verifying the ellipsoidal nature of the erosion process. Therefore, the area generated by each measured axis was calculated, and the difference between the two values was subtracted from the largest calculated area, thus providing the clearance area estimated for each jet, as shown in Table 2. Note, areas were calculated assuming a simple semi-circular shape for ease of calculation. The data in Table 2 indicate that the clearance area of the peripheral jets 1–6, are comparable, ranging from 0.33 – 0.39 m².

The central jet nozzle is positioned directly above the tank base, thus generates a circular profile hence the corresponding area was calculated as such. The clearance resulting from the longer jet firing duration in Regime 3 (0.79 m²), was markedly improved with respect to the shorter duration in Regime 2 (0.28 m²), suggesting that equilibrium erosion was not achieved in the latter scenario, an important result as the latter is indicative of operational procedure. Although increasing jet fire would improve the level of erosion (at least until maximum clearance is achieved according to the jet dimensions and flow velocity¹⁰ as attained in Regime 3) in the real HAST systems, fire time is limited by liquid volume in the jets. Given these limitations, the erosion data suggest that there will inevitably be regions where the bed remains unperturbed and thus full clearance is never achieved in the HASTs, which is in

agreement with the clearance model of McArthur *et al.*⁴², albeit the shape of the erosion patterns is different. One other potential reason for the low level of erosion is the influence of broad grain size distributions in the barytes, where the preferential transport of smaller particles may lead to larger particles armoring the bed, thus reducing erosion from jet scouring.^{6,9}

Sediment mobilization and dispersion in the FTR via different jet-fire sequences

The five second time averaged *G-function* [$G=\ln(\psi Vr)$] backscatter profiles of regimes 1 and 2 are presented in Figure 11A, for the 1 MHz data, and Figure 11B, for the 2 MHz data. Since the probes were offset in the rig, the listed distances for the 2 MHz in Fig. 11B are converted to be shown in respects of the 1 MHz probe, for consistency with the 1 MHz data. The position of the sharp peaks located at 0.75 m shifts by a few centimeters with respective regimes, suggesting that they denote the position of an eroding sediment bed, rather than the tank base itself. The R1 profile corresponds with measurement directly following the simultaneous prolonged operation (40 minutes) of jet 1 and the central jet. R2 profiles denote measurement at three time intervals in the final cycle of sequential jet operation in short bursts (20 seconds). Specifically, R2.1, R2.2 and R2.3 profiles correspond with measurements directly following the cessation of jet 2, jet 3 and jet 4 respectively (refer back to Table 1). The position of the transducers in relation to the jets is referenced in Figure 5.

The R1 profile in Figure 11A exhibits an intermediate intensity, which is assumed to be a consequence of mobilization of some sediment from the neighboring jet 1 and central jet regions, into the 1 MHz measurement zone. This is not the case for the 2 MHz profile in Figure 11B, since the corresponding transducer is positioned further

away from jet 1. The backscatter attenuation versus range is minor in both cases, indicating only dilute dispersion concentrations.⁴⁸ This result suggests that despite the long firing cycle, dispersion of sediment beyond localized regions is significantly hindered by the obstruction of the cooling coils, especially around the central jet. Therefore, even though the central jet has potentially a higher erosion capacity than the peripherals (because of its single vertical impingement zone) mixing throughout the greater tank area is almost completely obstructed. The physical obstruction of the cooling coils is pictured in Figure 5B, a CAD schematic of the internal configuration, where it can be seen that the coils occupy a significant volume of the tank.

Profiles R2.1, R2.2 and R2.3 however, exhibit significantly enhanced backscatter attenuation in comparison to the R1 profile, which is assumed to be a consequence of sediment re-suspension via the jets operating in the ABS measurement zones. Initially in Figure 11A, the R2.1 profile has a clear increase in the *G-function* gradient, in comparison to the R1 data, inferring a concentration increase. Subsequently, the attenuation gradient and thus suspension concentration, is again increased in R2.2, which also depicts a broad peak at 0.25 m (highlighted in the figure by an arrow). By profile R2.3, the broad peak has shifted closer to the bed (arrow at 0.4 m). It is assumed these peaks denote the position of a diffuse scattering plane generated by the density contrast of a dilute and relatively concentrated suspension,^{31,33,34} akin to the laboratory settling tests. Essentially, the peak in R2.2 corresponds with the maximum sediment dispersion height achieved by jet operation alone, and the movement of the peak in R2.3 suggests rapid settling of the re-suspended sediment occurs shortly after jet operation, within that specific measurement zone.

The settling rate of the interface, calculated from the difference between the two peaks with respect to the measurement time interval was 0.8 mm/s. This rate is higher than the Stokes settling velocity (0.51 mm/s), but lower than the rate of 1.35 mm/s in the batch scale settling studies at 0.7 vol%, reported earlier. Such a reduction may be indicative that the localized tank regions measured have a slightly higher concentration, which would reduce settling rates though enhanced hindered settling effects. It is also possible that the particles are not aggregating to the same extent as in the small scale batch settling studies. These results may be expected from greater levels of particle segregation given the likely inhomogeneity of the tank mixing. Indeed, since the dispersion zone-supernatant interface is detected by the ABS at only ~0.7 m, which is much lower than the total fluid depth, it is clear that the jets are not suspending the particles completely through the tank volume. The rapid settling behavior, also highlights the importance of maintaining and optimizing jet operations in actual radioactive HASTs, which normally operate jets in 30 minute intervals.⁴²

The attenuation changes in each regime, were quantified in terms of concentration, via the reference relationship established in the barytes calibration in Figure 7. Specifically the *G-function* backscatter profiles were smoothed over five consecutive time and distance bins, to reduce influences from inherent noise fluctuations in the measured signal. The corresponding $\partial G/\partial r$ slopes, were subsequently calculated between transducer ranges 0.3 – 0.5 m, denoted as the upper-region (UR) for the 1 MHz data, and 0.55 – 0.68 m, denoted as the near-bed (NB) for both 1 MHz and 2 MHz data. A wider range was not selected for the near-bed calculations due to enhanced signal fluctuations closer to the bed. The corresponding concentrations are presented in a bar chart in Figure 12.

As expected from the profile observations discussed, dispersion concentration of R1 is minimal compared with R2 profiles, the former of which corresponds with sediment erosion in neighboring jet regions to the ABS measurement zones. Particle levels clearly increase from R2.1 to R2.2, and then appear to level off or reduce, depending on the relative location between the probe and the firing jet in R2.3. In particular the R2 profiles align with the rapid settling scenario discussed, whereby concentration in the upper-region successively recedes with increasing concentration in the near-bed. There is also an apparent discrepancy between estimated concentration in the near-bed between the 1 and 2 MHz transducers, in R2.2 and R2.3. It is assumed that these differences are due to the fact that the probes were not laterally co-located. As the 1 MHz probe was closer to jet 3, it measured enhanced particle levels at R2.2 which carried forward to R2.3. Once again, these results highlight the lack of overall mixing in the tank from jet operation alone, and considerable inhomogeneities in particle dispersion levels, where it appears the liquid jets are only able to mobilize suspensions within the vicinity of the jet itself, suggesting that the cooling coils act to dampen any larger scale turbulent mixing.

Influence of air-lifts on sediment mobilization and settling in the FTR.

The impact of air-lift operation with respect to suspension mixing was investigated and directly compared with the mixing achieved without their utilization. *G-function* backscatter profiles were obtained for Regime 3 (jet cycle described in Table 1), both with and without air-lift operation. The level of dispersion in each scenario, as a function of time, is compared in the corresponding attenuation profiles presented in Figure 13 (A) without, and (B) with air-lifts. Levels of attenuation exhibited in the upper-region via the 1 and 2 MHz transducers, and in the near-bed region via the 2

MHz transducer are compared. The 1 MHz probe exhibits lower values of attenuation than the 2 MHz, due to the longer wavelength.⁴⁵ Note, some fluctuations are observed in the initial data points of each profile, since the cessation of suspension turbulence following air-lift operation is gradual.

In Figure 13A, without air-lift operation, the 2 MHz attenuation values are systematically lower in the upper-region than the near-bed, inferring depth-wise concentration stratification. The values for both regions in the air-lift scenario in Figure 13B, are analogous however, indicating improved mixing and dispersion homogenization. The comparative magnitude of the attenuation values is also systematically lower in the air-lift case. It is probable that improved mixing would better disperse the particles throughout the whole of the tank volume, reducing the relative concentration in the zone measured by the probes. All profiles, both with and without air-lift operation, depict a general reduction in attenuation over time. This is indicative of bulk concentration recession as the sediment settles. Importantly, the gradient, which represents reduction over time, is comparatively shallow in the air-lift scenario, which suggests that particle re-settling is more gradual in the air-lift experiments. Indeed, visual observations of the tank confirmed a consistently turbid dispersion which gradually clarified with time, which is unlike the rapid bulk settling behavior witnessed during jet operation alone. Thus, air-lift operation results in more favorable mixing conditions and resettling durations.

Samples were withdrawn from the FTR at 0.15 m (near-bed zone) in order to compare the characterized concentrations at different times using the *G-function analysis method described*, with physical measurements. Figure 14 compares the sampled and characterized values obtained in both over time. Specifically, ABS concentrations were calculated using the measured range 0.1-0.2 m, whereas the

samples were withdrawn at a specific 0.15 m location from the base (refer to Figure 5). The concentrations characterized via the ABS data, align well the physical sample concentrations, further validating the *G-function* approach used.²² The slight discrepancy in data at longer time periods for the case without air-lift operation is assumed to come from the spatial differences between the techniques. As the sample was taken from a single position at 15 cm, the zonal suspension front may have dropped below this point at longer periods leading to a significant drop off in measured concentration. Because acoustic data represent an average distance (10–20 cm) from the tank base, this drop-off would be less evident. Figure 14 shows a drop in concentration with time which is more gradual in the air-lift scenario, as seen in Figure 13. Indeed, the bulk concentrations are markedly lower in the case of air-lift operation, confirming that the air-lifts are able to mix and homogenize the dispersions to a much greater extent than jet operation alone. The data also suggest that they do not actually increase the amount of sediment eroded, but only aid in secondary mixing (or else the bulk concentration would have increased). Overall, the results demonstrate that air-lift operation is key to achieving optimized dispersion and mixing of eroded sediment to prevent rapid re-settling.

Conclusion

A four tenths scale non-active impinging jet tank (FTR), the design of which is based on an operational Highly Active Storage Tank (HAST), was profiled via an acoustic backscatter system (ABS). Sediment erosion, mixing, mobilization and re-settling dynamics, were investigated with respect to jet ballast and air-lift operating regimes, to facilitate operational optimization within actual HAST systems. The acoustic response of a bidisperse barytes suspension was first calibrated in the laboratory,

and a linear relationship was extracted between the *G-function* backscatter attenuation obtained via the *Rice method*²² and concentration. This reference relationship mediated the characterization of depth-wise concentration changes within a laboratory scale settling test and within the dynamic FTR dispersion, where characterized values aligned well with extracted samples. The *Rice method*²² also facilitated the quantification of the frequency specific attenuation constants of the mineral, for the first time here. The quantified attenuation was greater for this sediment compared with larger glass bead and plastic particles previously investigated,²² due to the dominating influence of size related viscous absorption of the backscattered pulse.

The *in situ* ABS analysis of the FTR found sediment bed erosion via jet impingement to be inhomogeneous and incomplete in all cases. The obstruction of the cooling coils dampened the mobilization of eroded sediment during jet only operations, resulting in localized and stratified dispersion of sediment, and subsequently rapid re-settling of particles. The additional turbulence generated during air-lift operation, significantly reduced bulk concentration in the measured regions, due to improved mixing and non-localized sediment distribution (although did not enhance sediment erosion). Overall, this research has given important insight into dispersion dynamics with respect to applied operations, within a very complex jet impingement system, facilitating the design and optimization of jet mixing processes. The *in situ* ABS monitoring technique, which incorporates both the *G-function Rice method*²² and phenomenological analysis approaches,^{31,32} has been able to analyze systems that would be otherwise almost completely inaccessible, and characterize particle settling dynamics and concentration changes, in both small scale and large scale dispersions.

Acknowledgments

The authors would like to thank Steve Rawlinson from the National Nuclear Laboratory (NNL) for technical support during industrial experimentation, and George McArthur and Sellafield Ltd for providing general support on the project. This work was funded by the Engineering and Physical Sciences Research Council (EPSRC) UK and the Nuclear Decommissioning Authority (NDA) as part of an Industrial CASE Award. Dave Goddard from the NNL provided general supervisory support on behalf of the NDA.

Literature Cited

1. Hazlehurst T, Harlen O, Holmes M, Povey M. Multiple scattering in dispersions, for long wavelength thermoacoustic solutions. Paper presented at: J Phys Conf Ser.2014.
2. Challis RE, Povey MJW, Mather ML, Holmes AK. Ultrasound techniques for characterizing colloidal dispersions. *Rep Prog Phys*. 2005;68(7):1541-1637.
3. Hunter TN, Peakall J, Unsworth TJ, et al. The influence of system scale on impinging jet sediment erosion: Observed using novel and standard measurement techniques. *Chem Eng Res Des*. 2013;91(4):722-734.
4. Gauglitz PA, Fort JA, Wells BE, Chun J, Bamberger JA, Jenks JJ. *The Role of Cohesive Particle Interactions on Solids Uniformity and Mobilization During Jet Mixing: Testing Recommendations*. : Pacific Northwest National Laboratory;2010.
5. Hamm B, West W, Tatterson GB. Sludge suspension in waste storage tanks. *AIChE J*. 1989;35(8):1391-1394.
6. Merry J. Penetration of vertical jets into fluidized beds. *AIChE J*. 1975;21(3):507-510.
7. Feng H, Olsen MG, Liu Y, Fox RO, Hill JC. Investigation of turbulent mixing in a confined planar-jet reactor. *AIChE journal*. 2005;51(10):2649-2664.
8. Betancourt F, Bürger R, Diehl S, Farås S. Modeling and controlling clarifier–thickeners fed by suspensions with time-dependent properties. *Miner Eng*. 2014;62:91-101.

9. Epely-Chauvin G, De Cesare G, Schwindt S. Numerical modelling of plunge pool scour evolution in non-cohesive sediments. *Eng Appl Comp Fluid*. 2014;8(4):477-487.
10. Unger DR, Muzzio FJ. Laser-induced fluorescence technique for the quantification of mixing in impinging jets. *AIChE J*. 1999;45(12):2477-2486.
11. Finlayson BL. Field calibration of a recording turbidity meter. *CATENA*. 1985;12(2-3):141-147.
12. Lynch JF, Irish JD, Sherwood CR, Agrawal YC. Determining suspended sediment particle size information from acoustical and optical backscatter measurements. *Cont Shelf Res*. 1994;14(10-11):1139-1165.
13. Gartner JW, Cheng RT, Wang P-F, Richter K. Laboratory and field evaluations of the LISST-100 instrument for suspended particle size determinations. *Mar Geol*. 2001;175(1-4):199-219.
14. Chu CP, Ju SP, Lee DJ, Tiller FM, Mohanty KK, Chang YC. Batch settling of flocculated clay slurry. *Ind Eng Chem Res*. 2002;41(5):1227-1233.
15. Kaushal DR, Tomita Y. Experimental investigation for near-wall lift of coarser particles in slurry pipeline using γ -ray densitometer. *Powder Technol*. 2007;172(3):177-187.
16. Hernando L, Omari A, Reungoat D. Experimental study of sedimentation of concentrated mono-disperse suspensions: Determination of sedimentation modes. *Powder Technol*. 2014;258:265-271.
17. Hubner T, Will S, Leipertz A. Sedimentation image analysis (SIA) for the simultaneous determination of particle mass density and particle size. *Part Part Sys Char*. 2001;18(2).
18. Bolton GT, Bennett M, Wang M, et al. Development of an electrical tomographic system for operation in a remote, acidic and radioactive environment. *Chem Eng J*. 2007;130(2-3):165-169.
19. Shukla A, Prakash A, Rohani S. Particles settling studies using ultrasonic techniques. *Powder Technol*. 2007;177(2):102-111.
20. Shukla A, Prakash A, Rohani S. Particle size distribution measurements in dense suspensions using ultrasonic spectroscopy with an improved model accounting for low angle scattering. *AIChE J*. 2010;10.
21. Shukla A, Prakash A, Rohani S. Online measurement of particle size distribution during crystallization using ultrasonic spectroscopy. *Chem Eng Sci*. May 2010;65(10):3072-3079.
22. Rice HP, Fairweather M, Hunter TN, Mahmoud B, Biggs S, Peakall J. Measuring particle concentration in multiphase pipe flow using acoustic backscatter: Generalization of the dual-frequency inversion method. *J Acoust Soc Am*. 2014;136(1):156-169.
23. Stener JF, Carlson JE, Pålsson BI, Sand A. Evaluation of the applicability of ultrasonic velocity profiling in conditions related to wet low intensity magnetic separation. *Miner Eng*. 2014;62:2-8.

24. Zou X-j, Ma Z-m, Zhao X-h, Hu X-y, Tao W-l. B-scan ultrasound imaging measurement of suspended sediment concentration and its vertical distribution. *Meas Sci Technol*. 2014;25(11):115303.
25. Norisuye T. Structures and dynamics of microparticles in suspension studied using ultrasound scattering techniques. *Polym Int*. 2016;Accepted.
26. Weser R, Woeckel S, Wessely B, Steinmann U, Babick F, Stintz M. Ultrasonic backscattering method for in-situ characterisation of concentrated dispersions. *Powder Technol*. 2014;268:177-190.
27. Rose CP, Thorne PD. Measurements of suspended sediment transport parameters in a tidal estuary. *Cont Shelf Res*. 2001;21(15):1551-1575.
28. Thorne PD, Hanes DM. A review of acoustic measurement of small-scale sediment processes. *Cont Shelf Res*. 2002;22(4):603-632.
29. Zhang W, Zhu Q, Hu J, Gu J, Yang S. Experimental Study of the Multifrequency Acoustic Backscatter System using Field Sediment. *Universal J Geosci*. 2015;3(6):188-194.
30. Fuller CB, Bonner JS, Islam MS, Ojo T, Page CA, Kirkey WD. Estimating Colloidal Concentration Using Acoustic Backscatter. *IEEE Sens J*. 2013;13(11):4546-4555.
31. Bux J, Peakall J, Biggs S, Hunter TN. In situ characterisation of a concentrated colloidal titanium dioxide settling suspension and associated bed development: Application of an acoustic backscatter system. *Powder Technol*. 2015;284:530-540.
32. Hunter TN, Darlison L, Peakall J, Biggs S. Using a multi-frequency acoustic backscatter system as an in situ high concentration dispersion monitor. *Chem Eng Sci*. 2012;80(0):409-418.
33. Carlson JE, Stener J, Sand A, Pålsson BI. Monitoring local solids fraction variations in multiphase flow using pulse-echo ultrasound. *Phys Procedia*. 2015;70:376-379.
34. Hunter TN, Peakall J, Biggs S. An acoustic backscatter system for in situ concentration profiling of settling flocculated dispersions. *Miner Eng*. 2012;27-28:20-27.
35. Stener JF, Carlson JE, Sand A, Pålsson BI. Monitoring mineral slurry flow using pulse-echo ultrasound. *Flow Meas Instrum*. 2016;50:135-146.
36. Kosior D, Ngo E, Dabros T. Determination of Settling Rate of Aggregates using Ultrasound Method during Paraffinic Froth Treatment. *Energ Fuel*. 2016;doi: 10.1021/acs.energyfuels.6b01714.
37. Betteridge KFE, Thorne PD, Cooke RD. Calibrating multi-frequency acoustic backscatter systems for studying near-bed suspended sediment transport processes. *Cont Shelf Res*. Feb 1 2008;28(2):227-235.
38. Thorne PD, Meral R. Formulations for the scattering properties of suspended sandy sediments for use in the application of acoustics to sediment transport processes. *Cont Shelf Res*. Feb 2008;28(2):309-317.

39. Moate BD, Thorne PD. Interpreting acoustic backscatter from suspended sediments of different and mixed mineralogical composition. *Cont Shelf Res.* 2011(0).
40. Downing A, Thorne PD, Vincent CE. Backscattering from a suspension in the near field of a piston transducer. *J Acoust Soc Am.* 1995;97(3):1614-1620.
41. Paul N, Biggs S, Edmondson M, Hunter TN, Hammond RB. Characterising highly active nuclear waste simulants. *Chem Eng Res Des.* 2013;91(4):742-751.
42. McArthur GAH, Tinsley TP, McKendrick D. Development of a liquid jet sludge re-suspension model (used on pulse jets or jet ballasts). Paper presented at: AIChE Annual Meeting 2005; Cincinnati, OH, USA.
43. Haynes WM. *CRC handbook of chemistry and physics*: CRC press; 2014.
44. Moore SA, Le Coz J, Hurther D, Paquier A. Using multi-frequency acoustic attenuation to monitor grain size and concentration of suspended sediment in rivers. *J Acoust Soc Am.* 2013;133(4):1959-1970.
45. Temkin S. *Suspension Acoustics: An Introduction of the Physics of Suspensions*: Cambridge University Press; 2005.
46. Johnson M, Peakall J, Fairweather M, Biggs S, Harbottle D, Hunter TN. Characterisation of multiple hindered settling regimes in aggregated mineral suspensions. *Ind Eng Chem Res.* 2016; 55(37): 9983-9993.
47. Balastre M, Argillier JF, Allain C, Foissy A. Role of polyelectrolyte dispersant in the settling behaviour of barium sulphate suspension. *Colloid Surface A.* 2002;211(2-3):145-156.
48. Rice HP, Fairweather M, Peakall J, Hunter TN, Mahmoud B, Biggs SR. Particle concentration measurement and flow regime identification in multiphase pipe flow using a generalised dual-frequency inversion method. *Procedia Eng.* 2015;102:986-995.

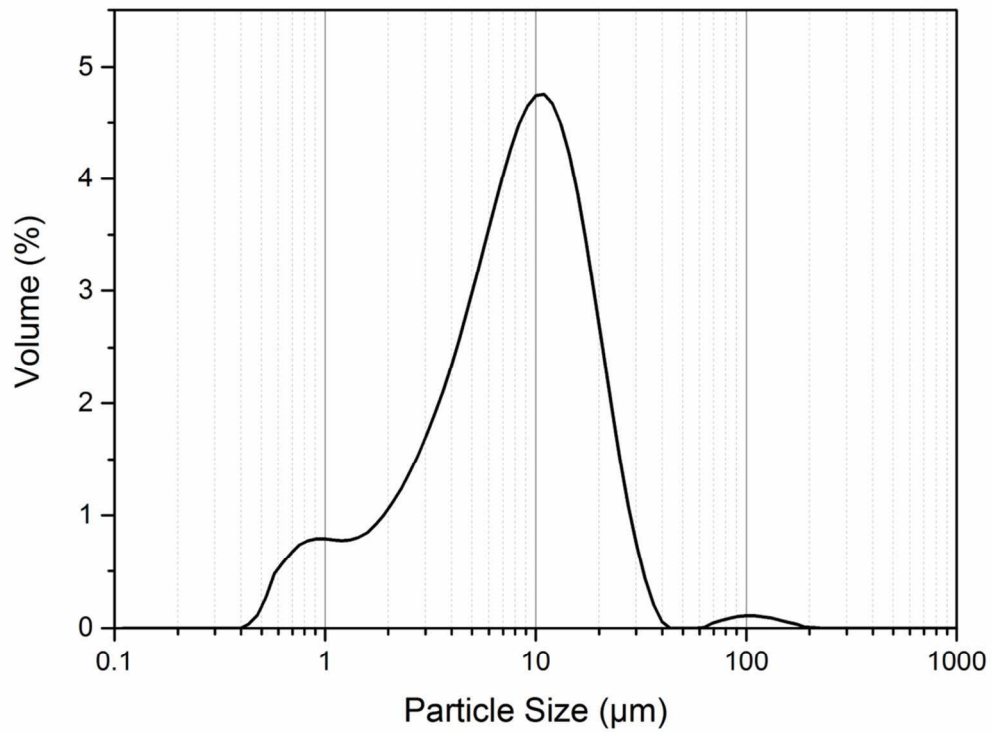


Figure 1. Particle size distribution of barytes sediment.

Figure 1
116x88mm (300 x 300 DPI)

Accep1

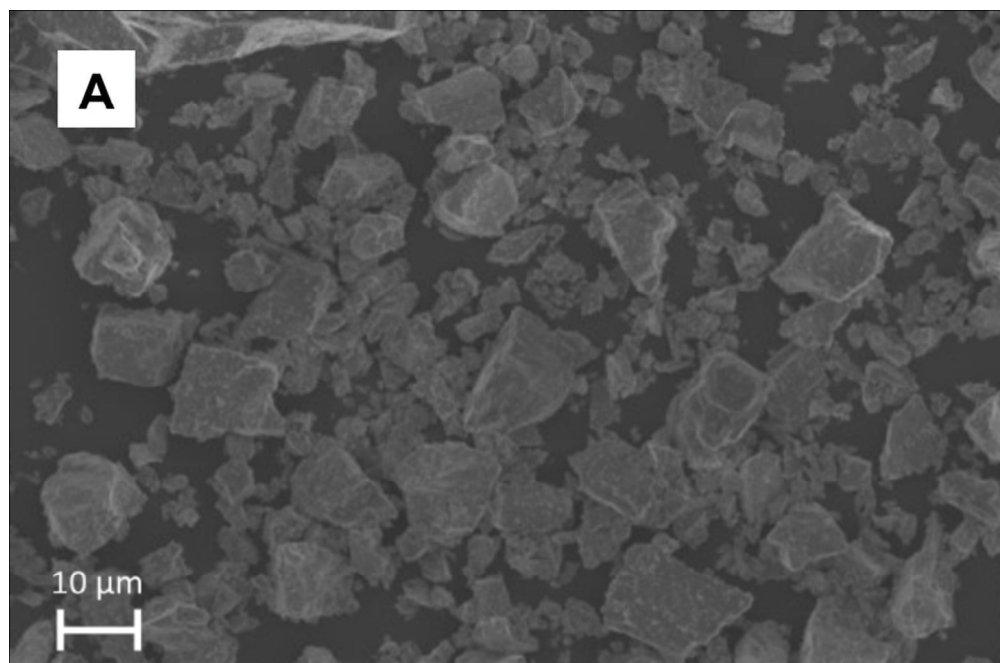


Figure 2. SEM micrographs of barytes sediment at (A) x 2,500 magnification and (B) x 10,000 magnification.

Figure 2A

77x50mm (300 x 300 DPI)

Accepte

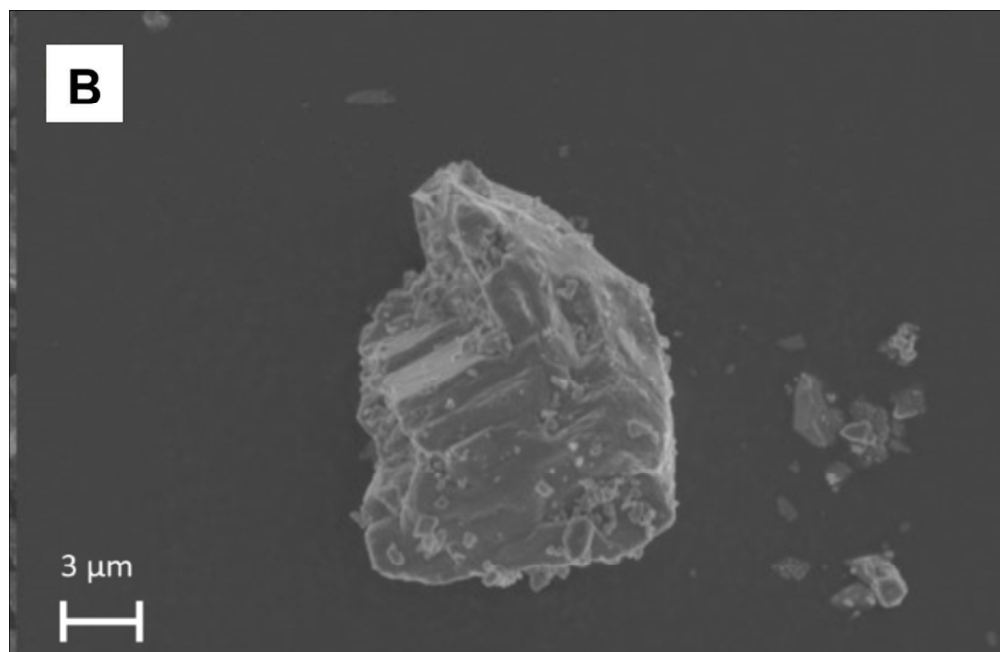


Figure 2. SEM micrographs of barytes sediment at (A) x 2,500 magnification and (B) x 10,000 magnification.

Figure 2B

78x50mm (300 x 300 DPI)

Accepte

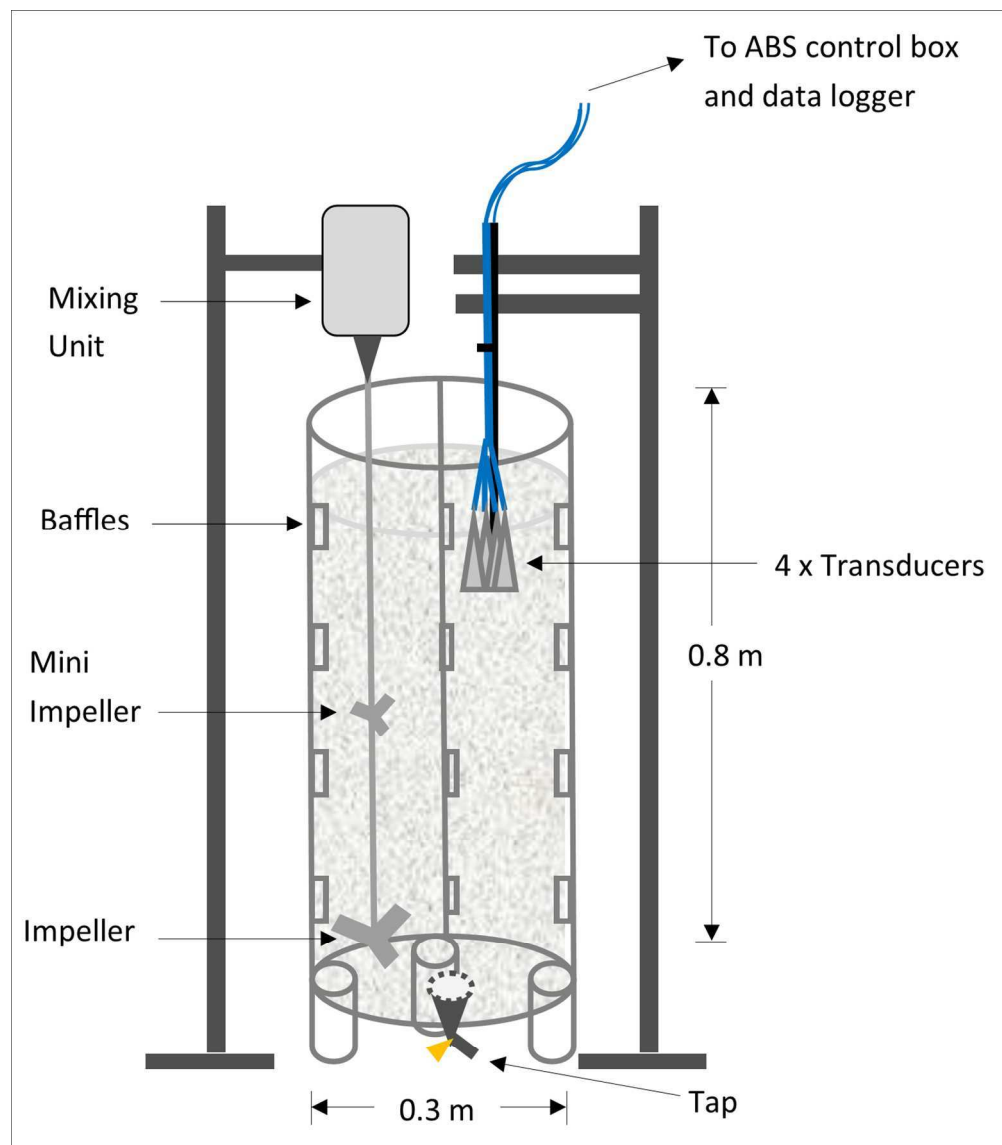


Figure 3. Experimental schematic of the acoustic calibration of barytes dispersions.

Figure 3

127x144mm (300 x 300 DPI)

AC

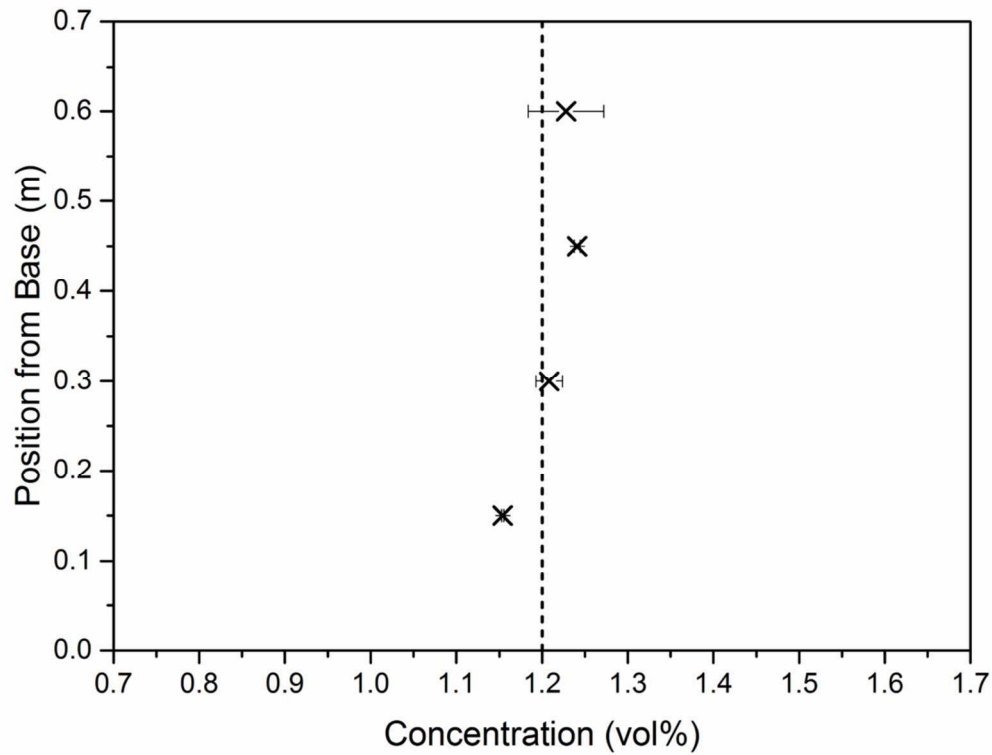


Figure 4. Dispersion homogeneity test conducted under calibration parameters and initial bulk concentration of 1.2 vol%.

Figure 4
117x91mm (300 x 300 DPI)

Accep

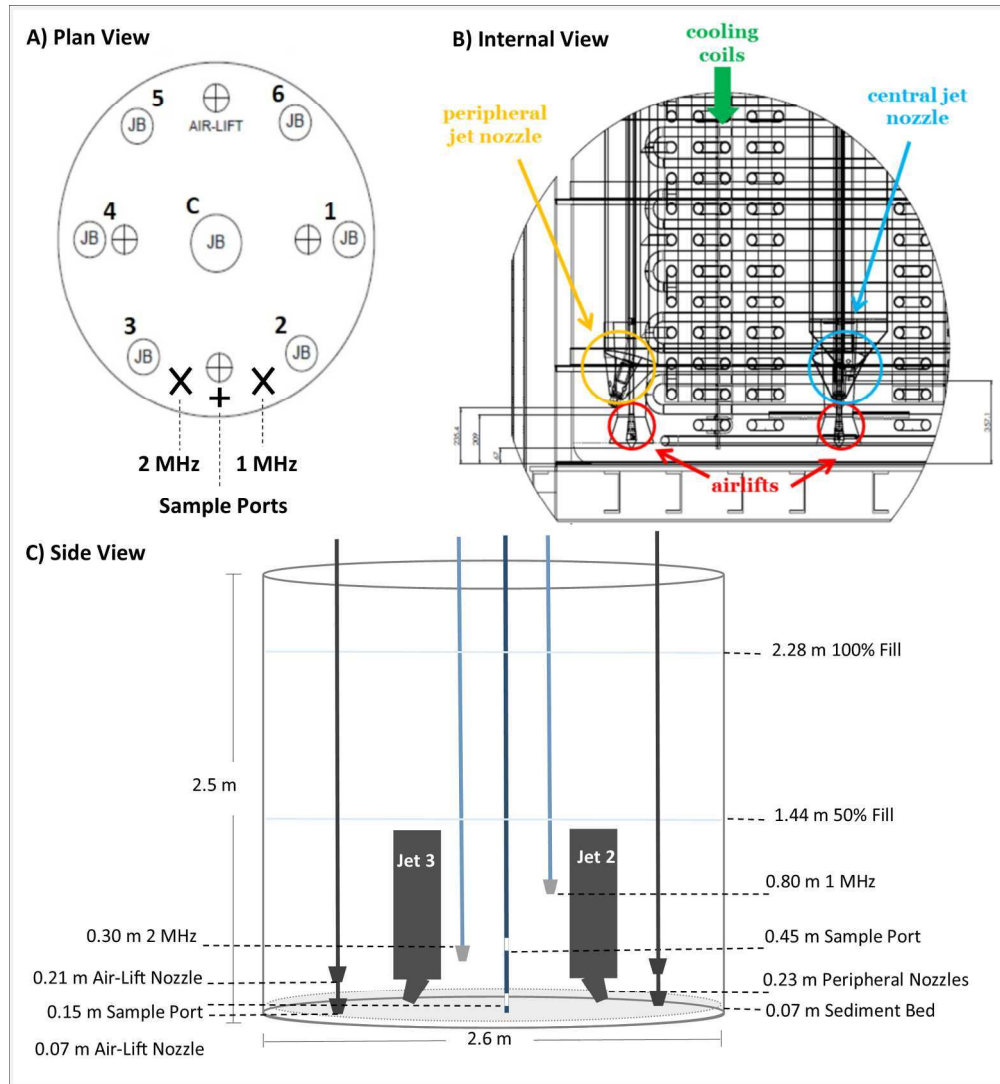


Figure 5. (A) Plan view, (B) CAD schematic of internal structure, and (C) side view of experimental configuration, (not drawn to scale and sediment drawn schematically as uniform).

Fig. 5
180x195mm (300 x 300 DPI)

Acc

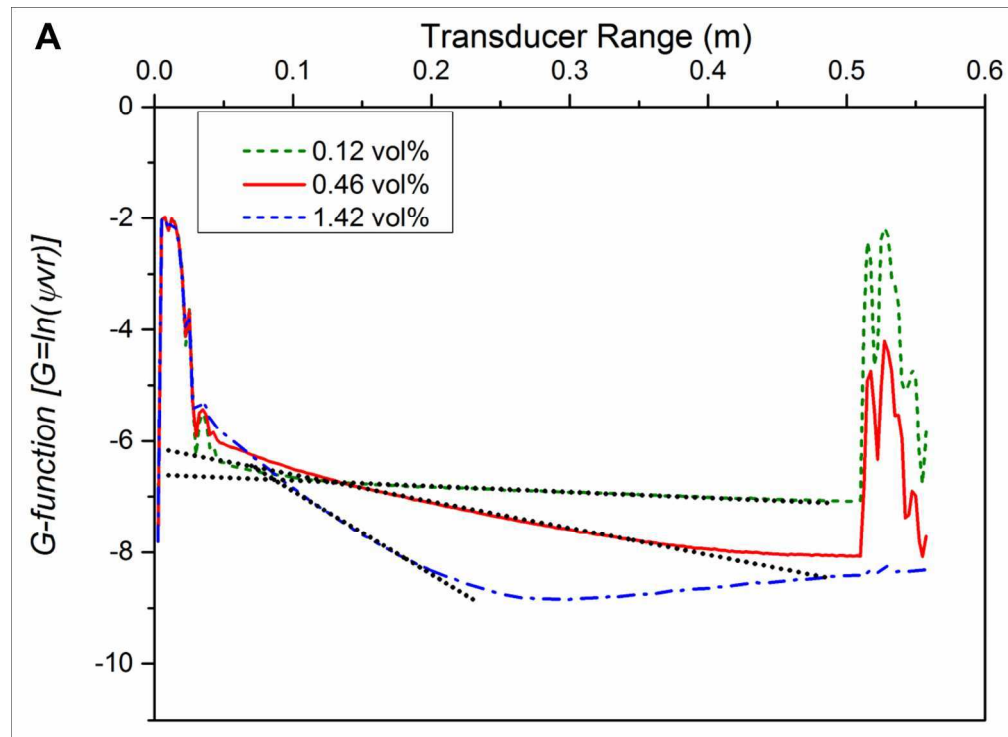


Figure 6. Average G-function $[G = \ln(\psi Vr)]$ backscatter profiles with respect to transducer range via (A) 1 MHz, and (B) 2 MHz, where the dashed lines represent linear gradient range. The average of the two 2 MHz probes is used in B.

Figure 6A
155x114mm (300 x 300 DPI)

Accep

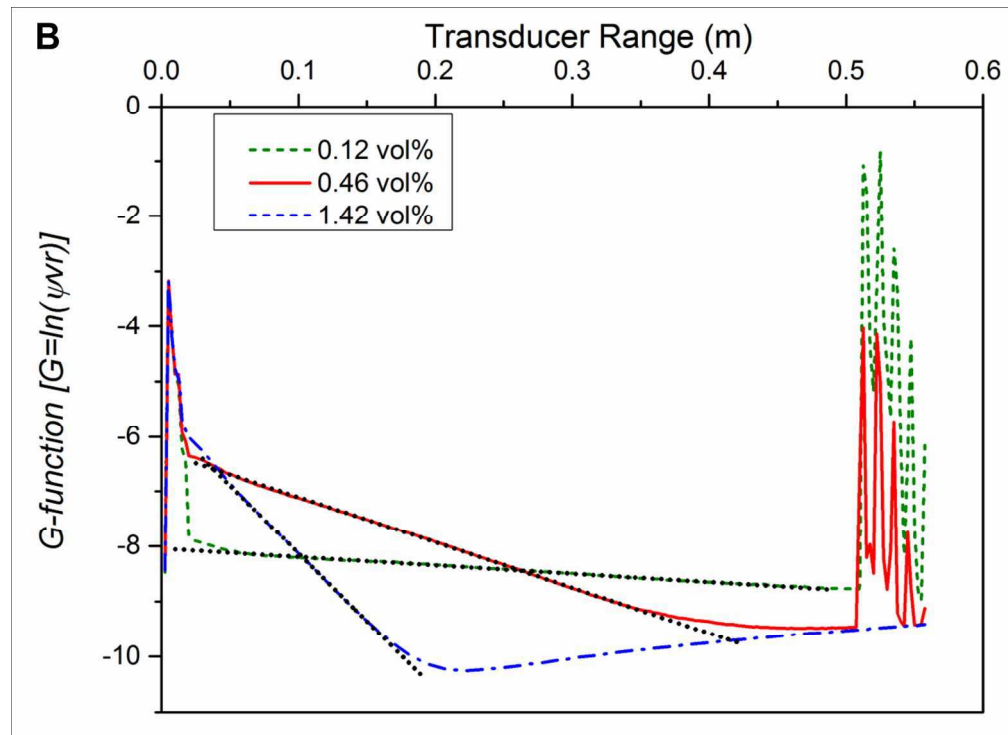


Figure 6. Average G-function $[G = \ln(\psi Vr)]$ backscatter profiles with respect to transducer range via (A) 1 MHz, and (B) 2 MHz, where the dashed lines represent linear gradient range. The average of the two 2 MHz probes is used in B.

Figure 6B
157x115mm (300 x 300 DPI)

Accepted

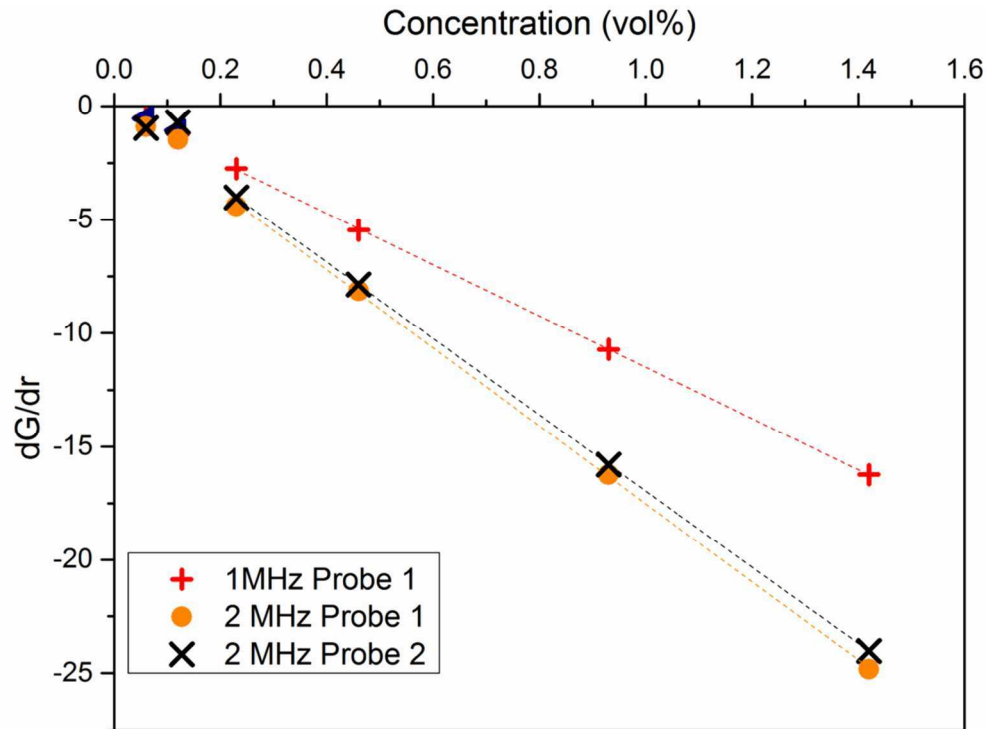


Figure 7. Barytes calibration reference relationship; dG/dr against M for each transducer.

Figure 7

113x84mm (300 x 300 DPI)

Accept

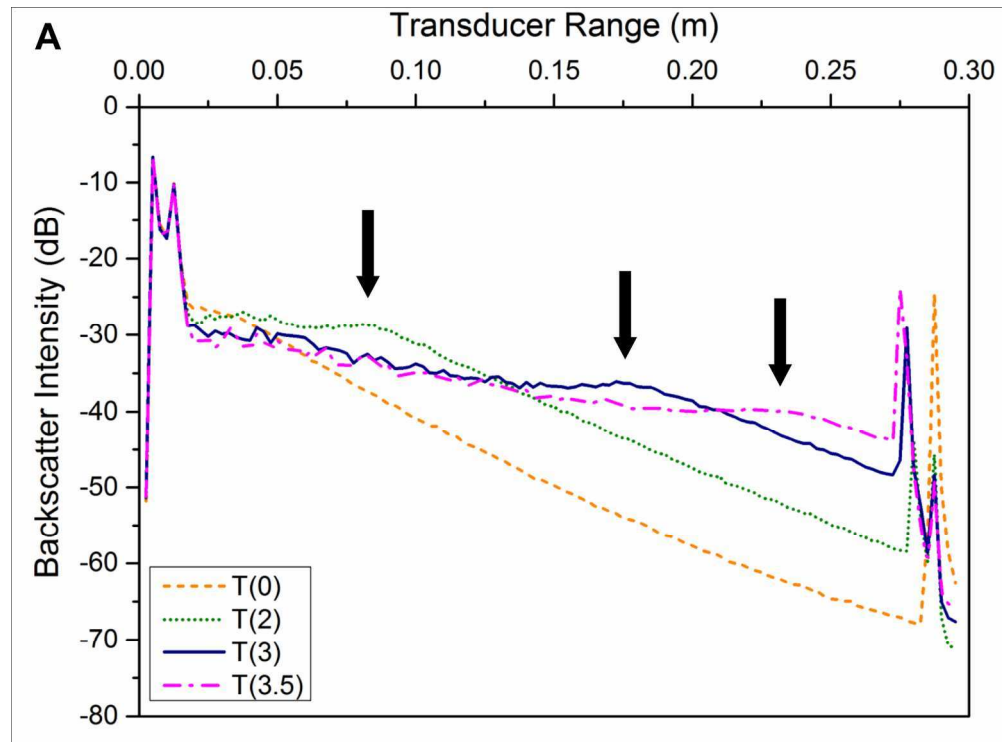


Figure 8. (A) 2 MHz time averaged backscatter profiles at time in minutes $T(\text{min})$, where arrows denote position of settling front, and (B) corresponding sedimentation curve; for 0.7 vol% dispersion.

Figure 8
155x114mm (300 x 300 DPI)

Accep1

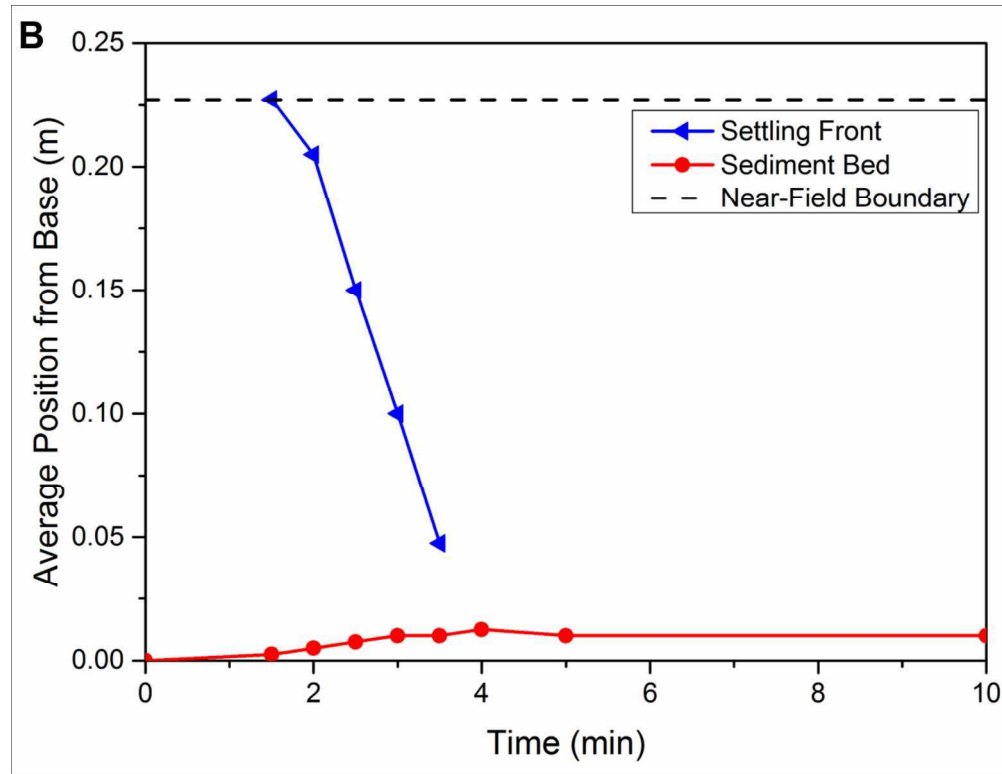


Figure 8. (A) 2 MHz time averaged backscatter profiles at time in minutes $T(\text{min})$, where arrows denote position of settling front, and (B) corresponding sedimentation curve; for 0.7 vol% dispersion.

Figure 8B

153x118mm (300 x 300 DPI)

Accep

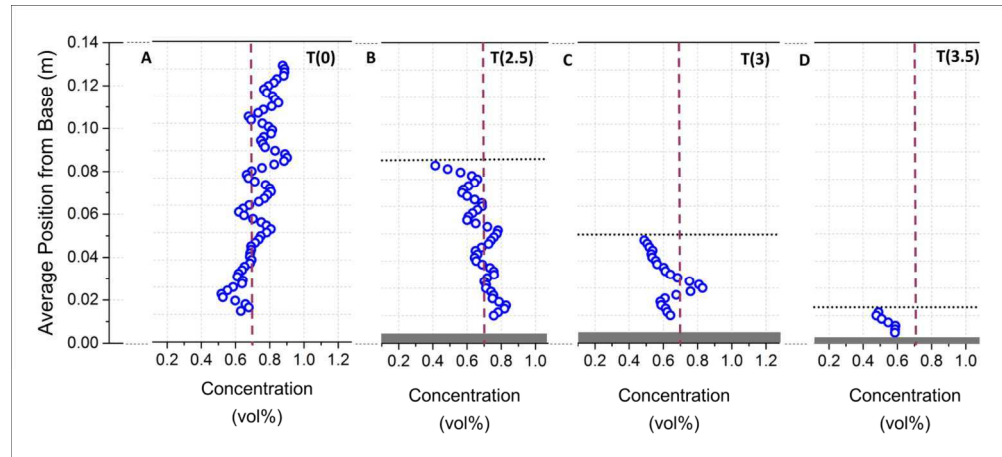


Figure 9. Concentration changes in settling dispersion with respect to depth at selected time profiles, for initial nominal bulk concentration of 0.7 vol% at; (A) start, (B) 2.5 minutes, (C) 3 minutes and (D) 3.5 minutes. Note the vertical lines indicate the initial bulk volume fraction, the horizontal line denotes the settling front position, and the shaded area represents the bed region.

Figure 9
192x87mm (300 x 300 DPI)

Accepted

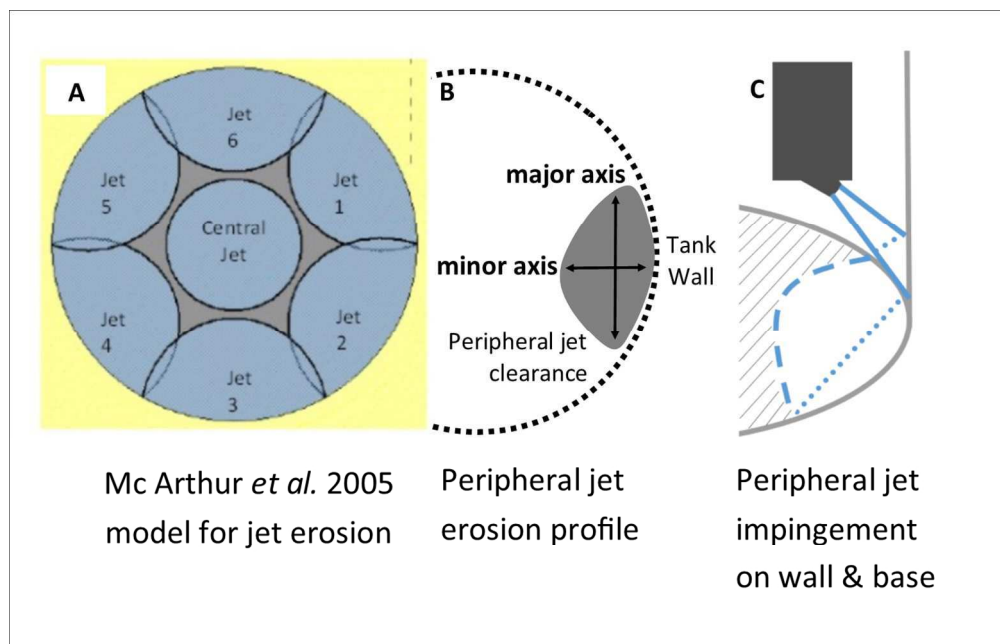


Figure 10. (A) Jet clearance pattern adapted from McArthur *et al.* (2005), (B) approximate shape of cleared sediment by peripheral jet, and (C) illustration of peripheral jet impingement on side wall, and secondary impingement on base.

Fig. 10
126x80mm (300 x 300 DPI)

Accept

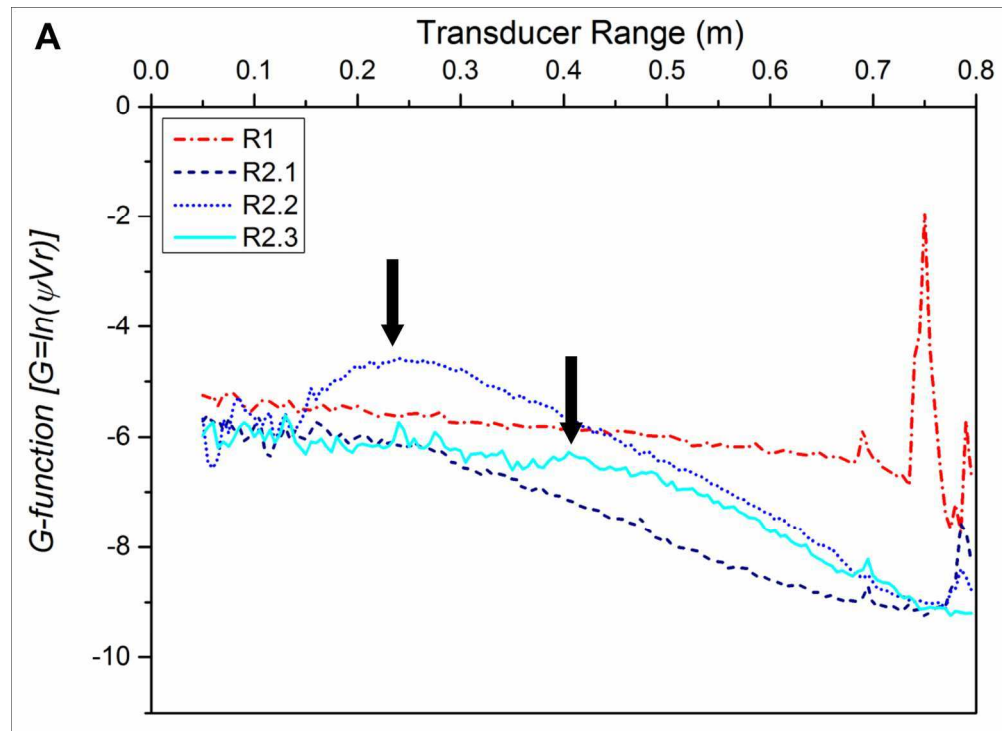


Figure 11. Time averaged G-function backscatter profiles obtained via (A) 1 MHz (where arrows indicate position of settling front boundary), and (B) 2 MHz R1 corresponds with measurement post Jet 1 + Central Jet operation. R2.1-3 correspond with measurements at three time intervals, post full jet cycle operation (refer to Table 1 for details).

Figure 11A

156x113mm (300 x 300 DPI)

Accep

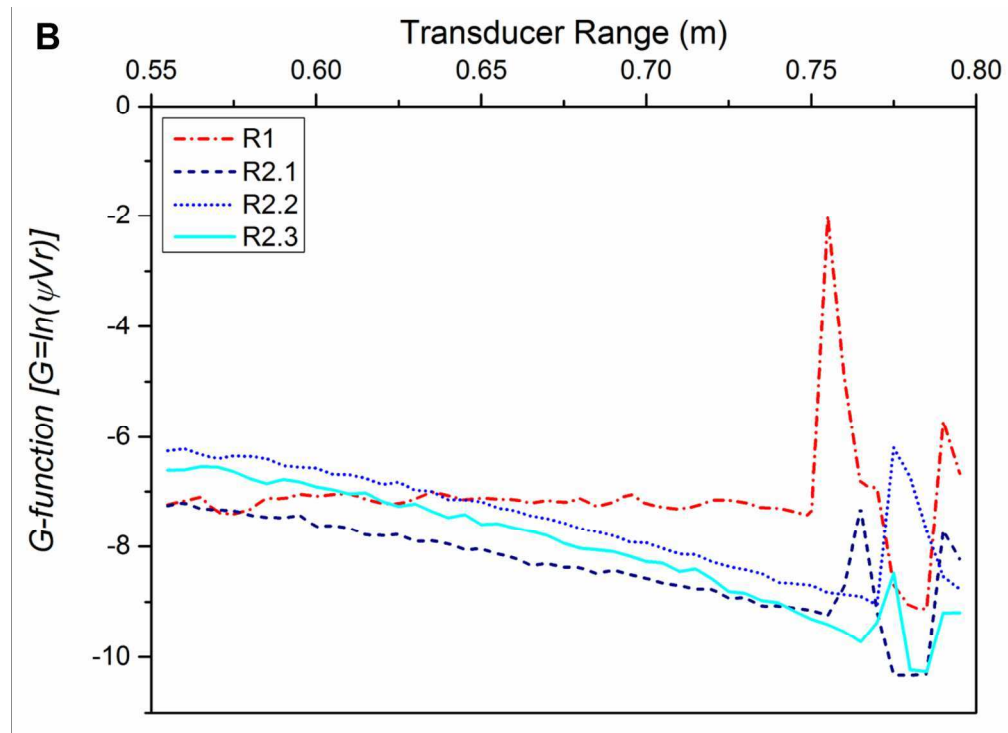


Figure 11. Time averaged G-function backscatter profiles obtained via (A) 1 MHz (where arrows indicate position of settling front boundary), and (B) 2 MHz R1 corresponds with measurement post Jet 1 + Central Jet operation. R2.1-3 correspond with measurements at three time intervals, post full jet cycle operation (refer to Table 1 for details).

Figure 11B

156x114mm (300 x 300 DPI)

Accep

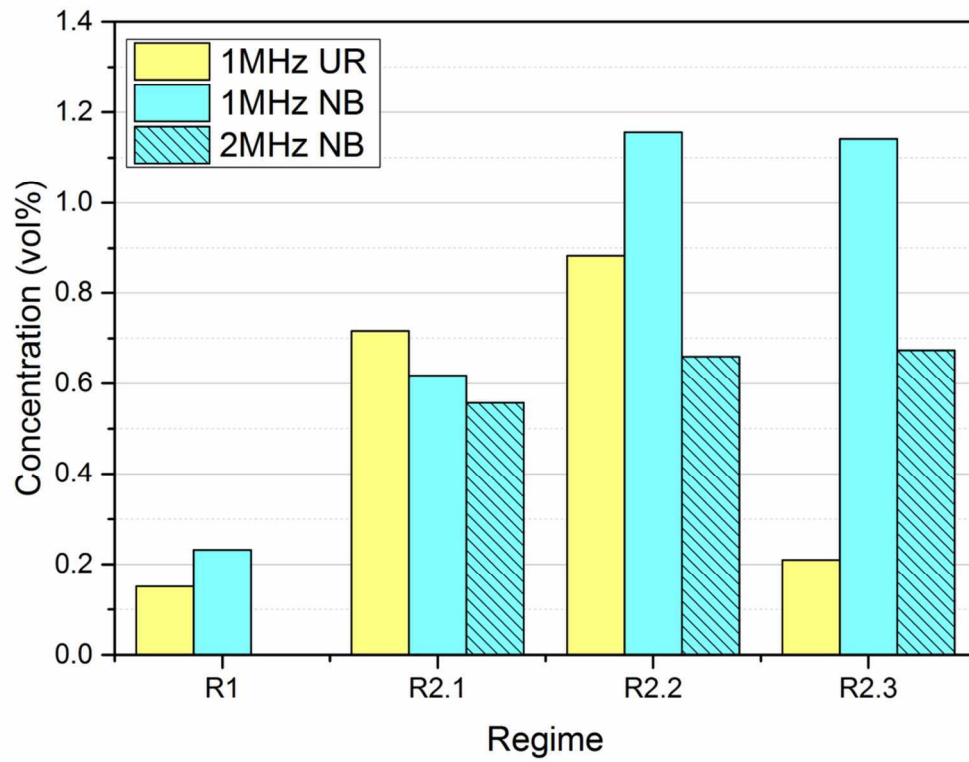


Figure 12. Concentration change per regime measured in the upper-region (UR) and near-bed (NB) with 1 and 2 MHz transducers.

Figure 12
117x91mm (300 x 300 DPI)

Accep

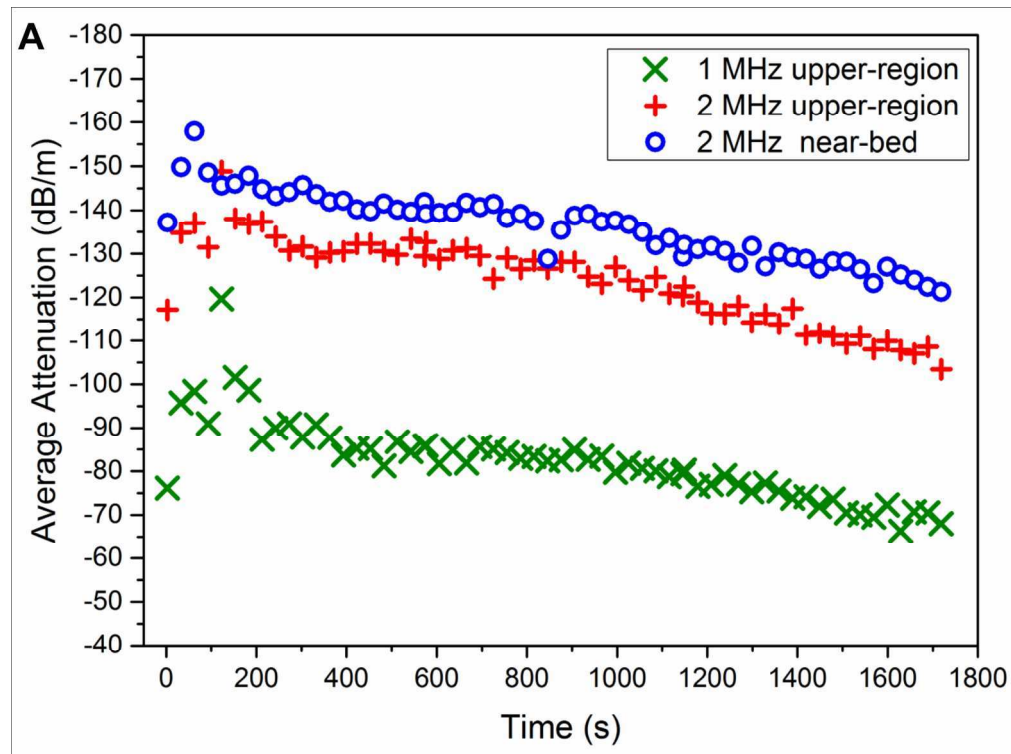


Figure 13. Average backscatter attenuation changes with time for Regime 3 in the upper-region measured via 1 and 2 MHz, and near-bed region measured by 2 MHz (A) without air-lift and (B) with air-lift operation. Each series represents measurements from an individual transducer.

Figure 13A

154x116mm (300 x 300 DPI)

Accep

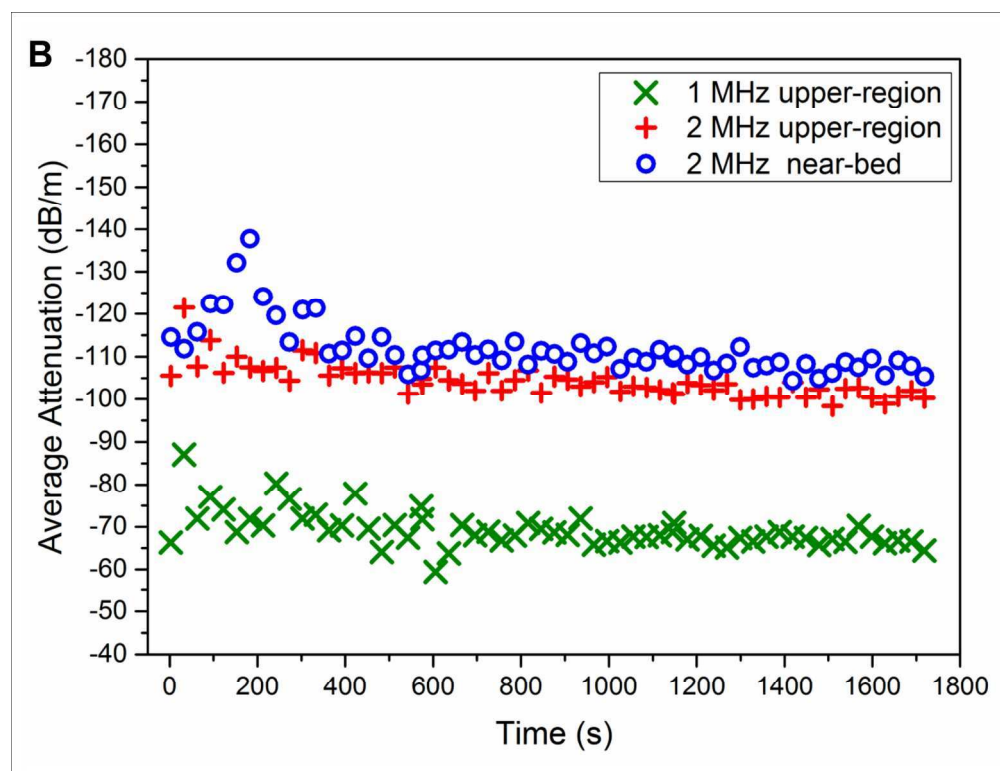


Figure 13. Average backscatter attenuation changes with time for Regime 3 in the upper-region measured via 1 and 2 MHz, and near-bed region measured by 2 MHz (A) without air-lift and (B) with air-lift operation. Each series represents measurements from an individual transducer.

Figure 13B
159x121mm (300 x 300 DPI)

Accep

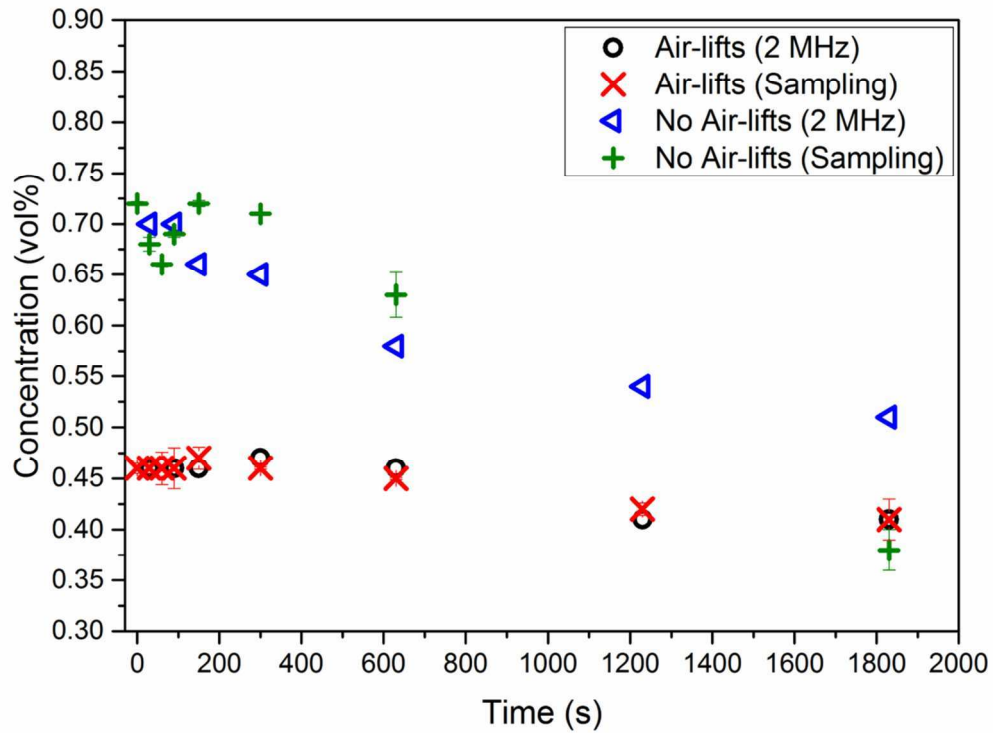


Figure 14. Comparison of concentration measured via ABS (2 MHz) and physical sampling in the near-bed region, with and without air-lift operation.

Figure 14

117x88mm (300 x 300 DPI)

Accepted

Table 1. Summary of experimental jet operating regimes employed in impinging jet ballast tank. The numbering of jets is shown in Figure 5.

Regime	Type	Jet Sequence	Burst Duration	Fill Level	Objectives
R1	ABS	1+C	40 min	50%	Erosion, neighboring jet influences, jet cycles, dispersion, re-settling
R2:	ABS	5+C, 1, 2 (R2.1), 3 (R2.2), 4 (R2.3)	20 s;	50%	
R2.1 ^a			100 s delay between jets		
R2.2 ^b					
R2.3 ^c					
R3:	ABS +	4, 5+C ^f , 6, 1, 2, 3	30 s;	100%	Assess air-lift influence; validate ABS concentrations with physical samples
R3.1 ^d	Sampling		no delay between jets		
R3.2 ^e					

^a ABS measurement commenced post firing of Jet 2.

^b ABS measurement commenced post firing of Jet 3.

^c ABS measurement commenced post firing of Jet 4.

^d No air-lifts operational.

^e All air-lifts continuously operated throughout regime.

^f Central jet continuously operated throughout regime.

Table 2. Summary of measured sediment clearance dimensions and associated clearance area estimated for each jet operating under Regime 3 (no air-lifts), and the central jet in Regime 2.

Jet	Duration (s)	Minor Axis (m)	Major Axis (m)	Estimated Clearance Area (m ²)
Central (continuous – R3)	720	0.50	-	0.79
Central (sequential – R2)	20 + 20	0.30	-	0.28
1	30	0.47	0.94	0.35
2	30	0.46	1.00	0.33
3	30	0.50	1.07	0.39
4	30	0.51	0.92	0.33
5	30	0.53	0.92	0.33
6	30	0.52	0.97	0.37